Measurement method for the nuclear anapole moment of laser-trapped alkali-metal atoms

E. Gomez,[1,*] S. Aubin,[1,†] G. D. Sprouse,[1] L. A. Orozco,[2] and D. P. DeMille[3]
[1]*Department of Physics and Astronomy, Stony Brook University, Stony Brook, New York 11794-3800, USA*
[2]*Department of Physics, University of Maryland, College Park, Maryland 20742-4111, USA*
[3]*Department of Physics, Yale University, New Haven, Connecticut 06520-8120, USA*
(Received 17 December 2004; revised manuscript received 16 May 2006; published 27 March 2007)

Weak interactions within a nucleus generate a nuclear spin dependent, parity-violating electromagnetic moment, the anapole moment. We analyze a method to measure the nuclear anapole moment through the electric dipole transition it induces between hyperfine states of the ground level. The method requires tight confinement of the atoms to position them at the antinode of a standing wave Fabry-Perot cavity driving the anapole-induced microwave $E1$ transition. We explore the necessary limits in the number of atoms, excitation fields, trap type, interrogation method, and systematic tests necessary for such measurements in francium, the heaviest alkali.

DOI: 10.1103/PhysRevA.75.033418 PACS number(s): 32.80.Pj, 32.70.Cs, 31.15.Ar

I. INTRODUCTION

Zel'dovich postulated in 1957 that the weak interactions between nucleons would generate a parity violating, time-reversal-conserving moment called the anapole moment [1]. Flambaum and Khriplovich calculated the effect it would have in atoms [2]. Experiments in thallium gave a limit for its value [3], and it was measured for the first time with an accuracy of 14% through the hyperfine dependence of atomic parity nonconservation (PNC) in cesium [4,5].

We present in this paper a measurement strategy of the nuclear anapole moment by direct excitation of the microwave electric dipole ($E1$) transition between the ground hyperfine levels in a chain of isotopes of an alkali-metal atom. Alkali-metal atoms are the best understood atoms quantitatively in their electronic properties associated with PNC. The precision of the Cs PNC experiments has required more detailed studies of the nuclear structure [6]. Measurements over a chain of isotopes offer the advantage that they can focus on the differences appearing as the number of neutrons changes. This task has been accomplished well by theory (see, for example, Ref. [7]) for the hyperfine anomaly measurements in Fr.

Current plans at the Isotope Separator and Accelerator (ISAC) at TRIUMF, in Vancouver, Canada, should provide access to all the neutron deficient long-lived isotopes of Fr with lifetimes above 30 s and to a similar number of the neutron rich isotopes, a sufficient variety to give a difference in number of neutrons of more than 10. The expected production rates should be at least two orders of magnitude larger than those obtained at Stony Brook, the leading place for study of Fr [8].

A measurement of the anapole moment in a chain of isotopes will provide information about neutral weak currents in the nucleus. The measurements can also give information on the nuclear structure and its changes as the number of neutrons increases [9,10].

The $E1$ transition between hyperfine levels is parity forbidden, but becomes allowed by the anapole induced mixing of levels of opposite parity. The general approach has been suggested in the past [11–18]. We would place many atoms inside a microwave Fabry-Perot cavity and hold them in a blue detuned dipole trap. The atoms would interact with the microwave field and with a Raman field generated by a pair of laser beams, in the presence of a static magnetic field. We would confine the atoms to the node (antinode) of the magnetic (electric) microwave field to drive only an $E1$ transition between hyperfine levels. The atoms would start in the lower hyperfine level, with the signal proportional to the population of atoms in the upper hyperfine level after the excitation. The interference with a Raman transition would give a signal linear in the $E1$ transition.

Recent work related to time-reversal invariance tests in atomic traps [19,20], points to the many advantages of combining traps with tests of fundamental symmetries, but also highlights the potential systematic errors present in such measurements, making a careful evaluation of the method prior to its implementation necessary. We focus our study primarily on isotopes of francium, the heaviest of the alkali-metal atoms [8], in an optical dipole trap, where the effect is expected to be large.

The organization of the paper is as follows: Section II gives the theoretical background for the nuclear anapole moment, Sec. III explains the proposed measurement method, Sec. IV presents an analysis of noise sources and systematic effects, and Sec. V contains the conclusions.

II. THEORETICAL BACKGROUND

The exchange of weak neutral currents between electrons and nucleons constitute the main source of parity-violating atomic transitions. The currents are of two kinds, depending on whether the electron or the nucleon enters as the axial vector current. The corresponding terms in the Hamiltonian

*Present address: National Institute of Standards and Technology, Maryland.
†Present address: Department of Physics, University of Toronto, Ontario, Canada.

differ on their dependence on the nuclear spin. The part independent of the nuclear spin is generally the dominant contribution in atomic PNC. This is not the case for the present work, where we consider transitions between hyperfine levels of the ground state, and the contribution from the nuclear spin-independent part is zero [21]. The Hamiltonian for the spin-dependent part in the shell model with a single valence nucleon of unpaired spin is given by [22]

$$H = \frac{G}{\sqrt{2}} \frac{K \boldsymbol{I} \cdot \boldsymbol{\alpha}}{I(I+1)} \kappa_i \delta(r), \tag{1}$$

where $G = 10^{-5} m_p^{-2}$ is the Fermi constant, m_p is the proton mass, $K = (I + 1/2)(-1)^{I+1/2-l}$, l is the nucleon orbital angular momentum, I is the nuclear spin, α are Dirac matrices, and κ_i is the interaction constant, with $i = p, n$ for a proton or a neutron. The terms proportional to the anomalous magnetic moment of the nucleons and the electrons have been neglected.

The interaction constant is given by [22]

$$\kappa_i = \kappa_{a,i} - \frac{K - 1/2}{K} \kappa_{2,i} + \frac{I+1}{K} K_{Q_W}, \tag{2}$$

with $\kappa_{2,p} = -\kappa_{2,n} = -1.25(1 - 4 \sin^2 \theta_W)/2$, corresponding to the tree level approximation, with $\sin^2 \theta_W \sim 0.23$ the Weinberg angle. Equation (2) has two corrections, $\kappa_{a,i}$ the effective constant of the anapole moment, and κ_{Q_W} that is generated by the nuclear spin-independent part of the electron nucleon interaction together with the hyperfine interaction. The three parts of this interaction constant can be traced to different ways in which the weak interacting vector boson Z^0 appears in the Feynman diagrams. The first one (the anapole) correspond to vertex corrections due to weak hadronic interactions on the nuclear side of the electromagnetic interaction coupled to the electron through a virtual photon. The second one takes the direct effect of a Z^0 exchange between the electron vector current and the nuclear axial current. The last one is the simultaneous exchange of a Z^0 and a photon modifying the hyperfine interaction. Flambaum and Murray showed that [22]

$$\kappa_{a,i} = \frac{9}{10} g_i \mu_i \frac{\alpha \mathcal{A}^{2/3}}{m_p \tilde{r}_0},$$

$$\kappa_{Q_W} = -\frac{1}{3} \left(\frac{Q_W}{\mathcal{A}} \right) \mu_N \frac{\alpha \mathcal{A}^{2/3}}{m_p \tilde{r}_0}, \tag{3}$$

where α is the fine structure constant, μ_i and μ_N are the magnetic moments of the external nucleon and of the nucleus, respectively, $\tilde{r}_0 = 1.2$ fm, $\mathcal{A}$ is the atomic mass number, Q_W is the weak charge, and g_i gives the strength of the weak nucleon-nucleus potential with $g_p \sim 4$ for a proton and $0.2 < g_n < 1$ for a neutron [23]. The anapole moment is the dominant contribution to the interaction in heavy atoms, for example, $\kappa_{a,p}/\kappa_{Q_W} \simeq 15$ for ^{209}Fr. We will assume from now on that $\kappa_i = \kappa_{a,i}$.

A. The anapole moment

The anapole moment of a nucleus is a parity nonconserving (PNC), time-reversal-conserving moment that arises from weak interactions between the nucleons (see the review by Haxton and Wieman [24].) It can be detected in a PNC electron-nucleus interaction, and reveals itself in the spin-dependent part of the PNC interaction. Wood *et al.* [4,5] measured the anapole moment of ^{133}Cs by extracting the dependence of atomic PNC on the hyperfine levels involved.

The anapole moment classically is defined by (see, for example, Ref. [25])

$$\mathbf{a} = -\pi \int d^3 r r^2 \mathbf{J}(\mathbf{r}), \tag{4}$$

with $\mathbf{J}$ is the electromagnetic current density [26]. The nuclear anapole moment in francium arises mainly from the weak interaction between the valence nucleons and the core. Flambaum, Khriplovich, and Sushkov [2] estimate the anapole moment from Eq. (4) for a single valence nucleon to be

$$\mathbf{a} = \frac{G}{e\sqrt{2}} \frac{K}{j(j+1)} \kappa_{a,i} \boldsymbol{j} = C_i^{an} \boldsymbol{j}, \tag{5}$$

where j is the nucleon angular momentum and e is the electron charge. The calculation assumes a homogeneous nuclear density, and a core with zero angular momentum, leaving the valence nucleon carrying all the angular momentum.

The measurement of the anapole moment gives information on the weak nucleon-nucleon interactions. A measurement of the anapole moment in a chain of isotopes would provide a separation of the anapole moment due to the valence proton or neutron.

B. Calculations of the anapole moment of francium isotopes

We use Eqs. (3) and (5) to estimate the anapole moment of five light francium isotopes with radioactive lifetimes longer than 1 minute [7]. The unpaired valence proton generates the anapole moment in even-neutron isotopes, whereas in the odd-neutron isotopes both the unpaired valence proton and neutron participate. Francium has an unpaired $h_{9/2}$ proton for all the isotopes and a $f_{5/2}$ neutron for the odd-neutron isotopes around ^{210}Fr. The protonic and neutronic contributions add vectorially to generate the anapole moment,

$$\mathbf{a} = \frac{C_p^{an} \boldsymbol{j}_p \cdot \boldsymbol{I} + C_n^{an} \boldsymbol{j}_n \cdot \boldsymbol{I}}{\boldsymbol{I}^2} \boldsymbol{I} = \frac{G}{e\sqrt{2}} \frac{(I+1/2)}{I(I+1)} \kappa_a \boldsymbol{I}, \tag{6}$$

with $C_i^{an} \boldsymbol{j}_i$ the anapole moment for a single valence nucleon i (proton or neutron) as given by Eq. (5) ($j_p = 9/2$, $j_n = 5/2$). Equation (6) defines the coupling strength of the total anapole moment (κ_a) resulting from adding the valence proton and neutron. Figure 1 shows the predicted values of κ_a for a string of francium isotopes [7] using $g_n = 1$.

C. Perturbation theory

The anapole moment induces a small mixing of electronic states of opposite parity. The effect of the anapole moment Hamiltonian on the ground state hyperfine levels according to first order perturbation theory is

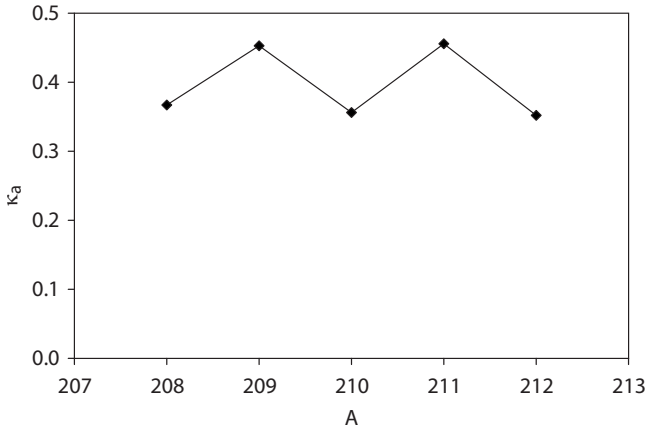

FIG. 1. Anapole moment effective constant for different isotopes of francium.

$$|\overline{sFm}\rangle = |sFm\rangle + \sum_{F'm'} \frac{\langle pF'm'|\mathbf{H_a}|sFm\rangle}{E_p - E_s}|pF'm'\rangle, \quad (7)$$

where E_p and E_s are the energies of the p and s states, respectively, and

$$\mathbf{H_a} = |e|\boldsymbol{\alpha}\cdot\mathbf{a}\delta(\mathbf{r}), \quad (8)$$

is the anapole moment Hamiltonian from Eq. (1), with $\mathbf{a}$ the anapole moment from Eq. (5). The matrix element in Eq. (7) gives [23]

$$\langle pF'm'|\mathbf{H_a}|sFm\rangle = i\frac{\xi Z^2 R}{(\varrho_s\varrho_p)^{3/2}}\frac{2\gamma+1}{3}\frac{(I+1/2)\kappa_a\mathcal{R}}{I(I+1)} \times[F(F+1)-I(I+1)-3/4]\delta_{F,F'}\delta_{m,m'}, \quad (9)$$

with $\xi = Gm_e^2\alpha^2/\sqrt{2}\pi = 3.651\times10^{-17}$, m_e the electron mass, Z the atomic number, ϱ_s and ϱ_p the effective principal quantum number for the s and p electronic states, $\gamma = \sqrt{(J+1/2)^2 - Z^2\alpha^2}$, J the electron total angular momentum, and $\mathcal{R}$ the Rydberg. The relativistic enhancement factor R is given by

$$R = 4(a_0/2Zr_0)^{2-2\gamma}/\Gamma^2(2\gamma+1), \quad (10)$$

with a_0 the Bohr radius, and $r_0 = \tilde{r}_0 A^{1/3}$.

The anapole moment mixes only states with the same F and m, and the mixing grows as $Z^{8/3}R$. For the ^{209}Fr ground state, we obtain

$$|\overline{sFm}\rangle = |sFm\rangle - i5.9\times10^{-13}\kappa_a\times[F(F+1)-25.5]|pFm\rangle. \quad (11)$$

The mixing coefficient is imaginary due to time-reversal symmetry. In practice, the mixing would be measured through the $E1$ transition amplitude A_{E1} [Eq. (16)] it induces between two hyperfine levels. The effect in francium is 11 times larger than in cesium [27].

III. PROPOSED MEASUREMENT STRATEGY

High efficiency magneto-optical traps (MOT) for francium atoms on line with an accelerator have been demonstrated [28]. Their performance and reliability matches the needs of the current proposed measurement strategy. Atoms captured on a first trap would then be transferred to a second MOT in a separate chamber. We would load the atoms into a dipole trap located at the electric field antinode of a standing wave in a microwave Fabry-Perot cavity. We would optically pump them into a single Zeeman sublevel, and prepare a coherent superposition of the hyperfine ground levels with a Raman pulse of amplitude A_R and duration t_R. Simultaneously we would drive the $E1$ transition of amplitude A_{E1} with the cavity microwave field, and measure the population in the upper hyperfine level (normalized to the total number of atoms $[N]$) using a cycling transition. The population in the upper hyperfine level at the end of each sequence would be

$$\Xi_\pm = N|c_e|^2 = N\sin^2\left(\frac{(A_R \pm A_{E1})t_R}{2\hbar}\right), \quad (12)$$

where c_e is the upper hyperfine level amplitude. The sign depends on the handedness of the coordinate system defined by the external fields, as explained in the next section. The signal for the measurement,

$$\mathcal{S} = \Xi_+ - \Xi_- = N\sin\left(\frac{A_R t_R}{\hbar}\right)\sin\left(\frac{A_{E1}t_R}{\hbar}\right) \simeq N\sin\left(\frac{A_R t_R}{\hbar}\right)\left(\frac{A_{E1}t_R}{\hbar}\right), \quad (13)$$

would be the difference between populations in the upper hyperfine level for both handedness. The last step assumes a small A_{E1}, the quantity proportional to the anapole moment constant κ_a.

A. Apparatus setup

Figure 2 shows a diagram of the proposed apparatus. The atoms would be placed inside a microwave Fabry-Perot cavity at the electric field antinode, confined in a blue detuned dipole trap to a volume with 10 μm length along the cavity axis, and a 1 mm diameter in the radial dimension. Observation of the electric dipole ($E1$) microwave transitions would be done through an interference method and extraction of the signal would require repeating the excitation varying the coordinate system.

Preparation of the atoms in a particular Zeeman sublevel of the lower hyperfine level $|F_1, m_1\rangle$ in an applied static magnetic field $\mathbf{B} = B_0\hat{\mathbf{z}}$ would be necessary. A resonant standing-wave microwave electric field $\mathbf{E}(t) = E\cos(2\pi\nu_m t + \psi)\cos(k_m y)\hat{\mathbf{x}}$ would excite the atoms to a particular Zeeman sublevel in the upper hyperfine level $|F_2, m_2\rangle$. The microwave magnetic field $\mathbf{M}$ would be aligned along $\mathbf{B}$, and it is $\pi/2$ out of phase (for a perfect standing wave) with $\mathbf{E}$ so that $\mathbf{M}(t) = M\sin(2\pi\nu_m t + \psi)\sin(k_m y)\hat{\mathbf{z}}$, with $M = E$ in cgs units.

The Raman transition would include two plane-wave optical fields, $\mathbf{E}_{R1}(t) = E_{R1}\cos(\omega_R t + \phi_R)\hat{\mathbf{x}}$ and $\mathbf{E}_{R2}(t)$

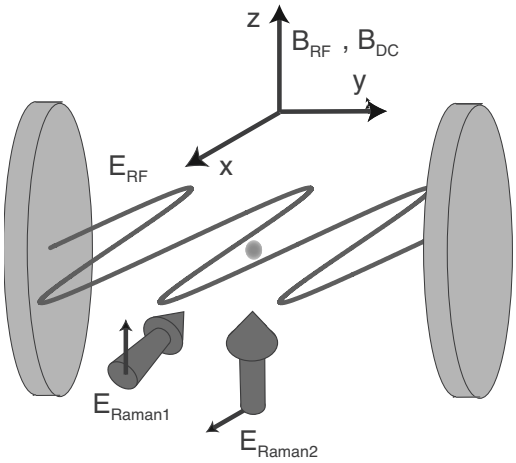

FIG. 2. Schematic setup of the proposed apparatus. The microwave cavity axis is along the y axis. The microwave electric field inside the cavity oscillates along the x axis. The two Raman laser beams are polarized along the x axis and z axis, respectively. The microwave magnetic field and the static magnetic field are both directed along the z axis. A dipole trap (not shown) holds the atoms at the origin that coincides with an antinode of the microwave electric field.

$=E_{R2}\cos[(\omega_R+2\pi\nu_m)t+\phi_R]\hat{\mathbf{z}}$, phase locked to the microwave field. The Raman carrier frequency ω_R would be tuned sufficiently far from optical resonance that only the vector part of the Raman transition amplitude $(\mathbf{V}\propto i\mathbf{E}_{R1}\times\mathbf{E}_{R2})$ would be non-negligible [29]; that is, we ignore the tensor part of the Raman amplitude.

B. Observable and reversals

The various electric and magnetic fields of the apparatus would define a coordinate system related to the measured rate $\Xi_{\pm}$. The transition rate $\Xi_{\pm}$ depends on three vectors: The polarization of the $E1$ transition $(\mathbf{E})$, the polarization of the Raman transition $(\mathbf{V})$, and the static magnetic field $\mathbf{B}$ that provides an axis for the spins of the nuclei. We combine these three vectors to produce the time-reversal preserving pseudoscalar $\mathbf{i(E\times(E}_{R1}\times\mathbf{E}_{R2})\cdot\mathbf{B})$, proportional to the measured quantity.

A single reversal of any of the fields in the above pseudoscalar changes the sign of the interference term of $\Xi_{\pm}$. We then would have the following reversals:

(1) Magnetic field reversal (β reversal).

(2) A shift of π in the relative phase between the $E1$ and the Raman fields (s reversal).

The Zeeman sublevels reverse with the magnetic field. The state preparation must be inverted in order to reach the correct Zeeman sublevel, meaning that σ^+ light goes into σ^- and vice versa. The magnitude of the static magnetic field and the microwave cavity frequency remain unchanged for this reversal.

C. Apparatus requirements

1. Magnetic field

We would drive $E1$ transitions between two particular Zeeman sublevels, $|F_1,m_1\rangle\rightarrow|F_2,m_2\rangle$ in different hyperfine levels of the ground state. While the frequencies of the exciting fields can be well controlled, the energy difference of the Zeeman states is determined primarily by the static magnetic field.

The experimental design should minimize the sensitivity to magnetic field fluctuations. The energy difference between two levels passes through a minimum at the static magnetic field B_0, and depends quadratically on the magnetic field around that point. We would use the Zeeman sublevels that give the smallest quadratic dependence. Table I lists the Zeeman sublevels and magnetic fields selected for different francium isotopes. The experiment would work between the $|F_1,m_1\rangle$ and $|F_2,m_2\rangle$ levels and also between the $|F_1,m_2\rangle$ and $|F_2,m_1\rangle$ levels, interchanging m_1 and m_2. The operating point of the static magnetic field and the frequency of the microwave cavity would have to be corrected slightly because of the nuclear spin contribution. The state preparation would also change to start in the appropriate level. The change of m_1 (m_2) for m_2 (m_1) does not work as a reversal because of the difference in transition amplitude, but it can still be useful as a consistency check.

The frequency for the $F=4$, $m=0$ to the $F=5$, $m=-1$ transition in ^{209}Fr, expanded around the critical field $B_0=1553$ G, is

$$\nu_m = 42.816\times10^9 + 90(B-B_0)^2 \text{ Hz}, \tag{14}$$

with B in G. Control of the magnetic field to 0.06 G (three parts in 10^5) reduces the frequency noise due to magnetic field fluctuations down to $\Delta\nu_m\sim0.3$ Hz.

The experiment would take place in a large magnetic field whereas the state preparation and detection occur in a small magnetic field. The transition between both regimes should

TABLE I. Parameters of the five relevant francium isotopes: Spin, hyperfine splitting (hfs) of the $7s_{1/2}$ state (Refs. [30] and [31]), Zeeman sublevels m_1, m_2, and their energy separation ν_m at the static magnetic field B_0 used in the proposed measurement.

Isotope	Spin	hfs (MHz)	m_1	m_2	B_0 (G)	ν_m (MHz)
208	7	49880.3	0.5	1.5	2386.5	49433
209	9/2	43033.5	0	−1	1553.0	42816
210	6	46768.2	0.5	1.5	2586.4	46208
211	9/2	43569.5	0	−1	1572.3	43349
212	5	49853.1	0.5	1.5	3265.7	49015

be done adiabatically. The time scale is determined by the precession time in a small magnetic field, resulting in a magnetic field ramp duration of hundreds of microseconds.

2. The microwave cavity

The francium hyperfine separation requires a Fabry-Perot microwave cavity operating at around 45 GHz (wavelength $\lambda_m \sim 0.66$ cm) in a Fabry-Perot configuration; for example, a cavity with a mirror separation of $d \sim 20\lambda_m \sim 13$ cm and a mirror radius of $r_m = 3.5$ cm. These parameters combine to minimize diffraction losses as the Fresnel number $F_N > 1$, where $F_N = r_m^2/\lambda_m d$ [32].

The quality factor (Q) of the cavity is

$$Q = \frac{d}{2\varsigma}, \tag{15}$$

where ς is the skin depth and is equal to $\sqrt{2/\omega\mu_0\sigma}$ with μ_0 the magnetic constant and σ the conductivity ($5.8 \times 10^7 \Omega^{-1}$ m^{-1} for copper at room temperature). The conductivity limited quality factor is $Q = 1.9 \times 10^5$. It is possible to couple 58 mW into the cavity with current available technology, which would give an electric field of 476 V/cm to drive the $E1$ transition.

The $E1$ transition amplitude for ^{209}Fr between the initial hyperfine level ($\bar{i}$) $F=4$, $m=0$ to the final hyperfine level ($\bar{f}$) $F=5$, $m=-1$ with a static magnetic field of 1553 G (see Table I) is

$$A_{E1}/\hbar = \langle \bar{f}| -e\mathbf{E}\cdot\mathbf{r}|\bar{i}\rangle/\hbar = 0.01i\left[\frac{E}{476\ \text{V/cm}}\right]\left[\frac{\kappa_a}{0.45}\right]\ \text{rad/s}. \tag{16}$$

A more accurate result can be obtained with the use of many-body perturbation theory [27,33,34].

A 1 cm cavity waist would cover the atoms in the 1 mm diameter 10 μm length trap, and radius of curvature of $R_m = 9.9$ cm for the cavity mirrors ensure a stable cavity, since $[1-(d/2R_m)]^2 < 1$. The curvature of the wave fronts could create a gradient of polarization of the microwave field smaller than 3×10^{-5} rad cm^{-1} over the volume of the trap. We show later that this rotation is within acceptable ranges.

The field inside the cavity can be decomposed into a standing wave and a traveling wave. The presence of the traveling wave generates $M1$ transitions despite the location of the atoms at the node of the standing wave magnetic field. Significant reduction of the amplitude of intracavity traveling waves comes with a symmetrical arrangement of identical antennas, one on each mirror. Antennas give a high coupling efficiency into the cavity [35] as compared to a slit or a grating [36]. The electric field inside the cavity is given by

$$E = e^{-i\nu_m t}\left(\frac{1}{1-r_1 r_2 e^{2ik_m d}}\right) \times [E_1 t_1 (e^{ik_m z} - r_2 e^{ik_m d} e^{-ik_m z}) + E_2 t_2 (e^{-ik_m z} - r_1 e^{ik_m d} e^{ik_m z})], \tag{17}$$

where r is the reflectivity, t the transmissivity, k is the wave vector of the microwave field, d the separation between the mirrors, and the subindices 1 and 2 refer to the two mirrors. The first (second) term is the field generated by antenna 1 (2). The expression is the sum of two waves, one traveling to the right and the other to the left. The difference in amplitude between these two contributions results in a traveling wave. The ratio of traveling to standing wave assuming a symmetrical cavity, that is $r_1 = r_2 = r$ and $t_1 = t_2 = t$, is

$$\mathcal{R}_{T/S} = \left(\frac{i\vartheta}{4} + \frac{E_1 - E_2}{4E_1}\right)[i(1-r) + k_m \Delta d], \tag{18}$$

with ϑ the phase mismatch from both antennas and Δd the deviation of the cavity mirrors separation from the ideal position. Assuming $\vartheta = 0$ and control of the amplitude from each antenna to 1%, the position of the mirrors to 0.1 μm and taking $1 - r = 3.6 \times 10^{-4}$ (consistent with the Q factor computed above), we obtain $\mathcal{R}_{T/S} = (3+9i) \times 10^{-7}$.

3. Dipole trap

We choose a far-detuned dipole trap to contain the atoms for the duration of the measurement since the perturbations introduced by it are small and measurable. A variety of different geometries have been proposed over the years. These include red-detuned traps based on focused beams, and blue-detuned traps with hollow beams (see Refs. [37] and [38] for reviews of recent work.)

The trap would confine the atoms within 10 μm around the microwave electric field antinode and 1 mm diameter in the radial dimension. The region of confinement would be smaller than the microwave wavelength (Lamb-Dicke regime), so Doppler broadening becomes negligible.

The ac Stark shift (ΔE), which produces the restoring force of the dipole trap, displaces the two hyperfine levels of ground state in the same direction but not by the same amount. The differential shift changes the resonant frequency for the cavity-driven $E1$ transition used in the anapole moment measurement. The change in the hyperfine separation for a detuning ($\delta = w - w_e$) larger than the hyperfine splitting (Δ_{hfs}) is approximately equal to ($\Delta_{\text{hfs}}/\delta$)$\Delta E$ [39]. The shift reduces considerably using a blue detuned far off resonance trap (FORT) at 532 nm.

The dipole trap in combination with the cavity field may generate a multiphoton transition. There are four vectors available for that transition: $\mathbf{E1_D}$, $\mathbf{M1_D}$ the dipole trap electric and magnetic fields, $\mathbf{E}$ the microwave electric field, and $\mathbf{B}$ the static magnetic field. The parity and time-reversal-conserving observables created with combinations of the above vectors that produce a resonant transition $((\mathbf{E1_D}\cdot\mathbf{E}) \times (\mathbf{M1_D}\cdot\mathbf{B})$, $(\mathbf{E1_D}\cdot\mathbf{B})(\mathbf{M1_D}\cdot\mathbf{E})$, $(\mathbf{E1_D}\times\mathbf{E})\cdot(\mathbf{M1_D}\times\mathbf{B})$, $(\mathbf{E1_D}\times\mathbf{B})\cdot(\mathbf{M1_D}\times\mathbf{E})$, $(\mathbf{E1_D}\times\mathbf{M1_D})\cdot(\mathbf{E}\times\mathbf{B})$, and $i(\mathbf{E1_D} \times\mathbf{E})\cdot\mathbf{M1_D})$, give a negligible contribution if the trap laser propagates along $\mathbf{B}$.

4. M1 transition

The dominant transition between the two hyperfine states is a magnetic dipole $M1$ transition. The magnetic component of the microwave field could drive $M1$ transitions. A microwave magnetic field polarized along the x axis would have the same signature as a parity-violating signal. The $M1$ tran-

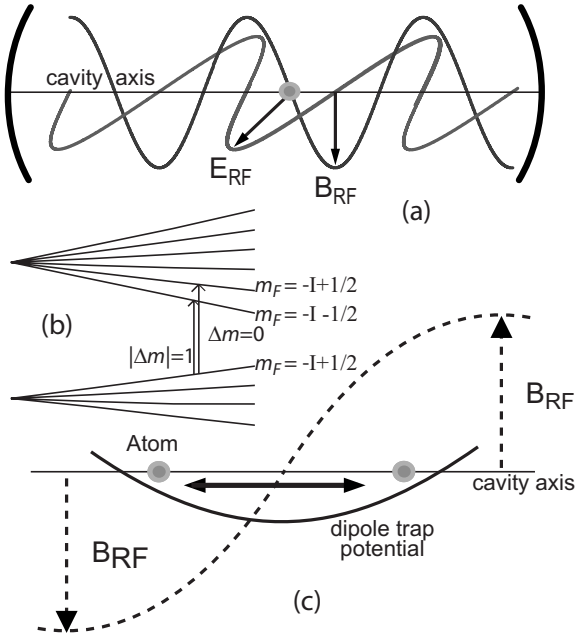

FIG. 3. Suppression mechanisms of the $M1$ transition. (a) Trapped atoms would sit at the magnetic field node, where the magnetic field is zero. (b) Schematic of the ground hyperfine levels showing a $|\Delta m|=1$ transition such as the one for the anapole moment and the $\Delta m=0$ out of resonance transition such as that induced by the $M1$ field. The level spacing as well as the spin do not correspond to any particular atom. (c) Trapped atoms would oscillate around the microwave magnetic field node and would sample a zero time-averaged magnetic field.

sition amplitude (A_{M1}) between the levels of interest is given by

$$A_{M1}/\hbar = \langle \bar{f}|(-e/2m_e)(\mathbf{J}+\mathbf{S})\cdot\mathbf{M}|\bar{i}\rangle/\hbar = 7.8\times 10^6\left[\frac{M}{1.6\ \mathrm{G}}\right]\ \mathrm{rad/s}, \quad (19)$$

for the maximum expected microwave magnetic field in the Fabry-Perot cavity. The ratio of the $E1$ transition [Eq. (16)] to the $M1$ transition is $|A_{E1}/A_{M1}|\sim 1\times 10^{-9}$. The success of the measurement depends on reducing and understanding this transition. We propose to suppress it in three ways.

First [see Fig. 3(a)], we would place the atoms at the magnetic field node (electric field antinode) of the microwave cavity. The magnitude of the microwave magnetic field at the edges of the atomic trap is reduced by a factor $\mathfrak{N}=\sin(2\pi d_t/\lambda_m)$, with $d_t=10$ μm the length of the trap along the cavity axis. The reduction factor at 45 GHz is $\mathfrak{N}=4.8\times 10^{-3}$.

Second [see Fig. 3(b)], we would direct the polarization of the $M1$ field to be along the z axis (Fig. 2). The nonresonant $M1$ transitions in this case would be of the type $\Delta m=0$. The static magnetic field (B_0) would split the Zeeman sublevels of the two hyperfine levels, and the microwave field would be resonant for the $|\Delta m|=1$ $E1$ transitions (the microwave electric field would be polarized along the x axis). The alignment imperfections give a suppression factor equal to $\sin(\phi)\sim\phi\sim 10^{-3}$ rad, the angle of the microwave magnetic field polarization with respect to the z axis.

Third [see Fig. 3(c)], the atoms in the dipole trap would oscillate around the microwave magnetic field node. An atom crossing the node would see a microwave magnetic field pointing in the opposite direction. The change in position effectively would flip the phase of the magnetic field that the atom sees, and would reverse the evolution generated by the $M1$ transition. The dynamical suppression only takes place if the frequency of oscillation (ζ) of the atoms inside the trap is larger than the Rabi frequency of the $M1$ transition and is given by $(1/\sqrt{N})\Omega_{M1}/\zeta$. The frequency of oscillation along the cavity axis for the proposed geometry would be $\zeta/2\pi\sim 300$ Hz.

Taken together, the three suppression mechanisms would reduce the expected $M1$ transition amplitude to $A_{M1s}/\hbar=1.9\times 10^{-5}$ rad/s for 10^6 atoms. This is 500 times smaller than the amplitude for the $E1$ transition.

D. Signal-to-noise ratio

The magnitude of the signal from Eq. (13) reaches a maximum for a Raman transition amplitude of $A_R=(2n+1)\pi/2$ with $t_R=1$. The measurement of the upper hyperfine state population collapses the state of each atom into one of the two hyperfine levels. The collapse distributes the atoms binomially between the two hyperfine levels and leads to an uncertainty in the measured excited state fraction called projection noise $\mathcal{N}_P$ [40]. The projection noise is given by

$$\mathcal{N}_P=\sqrt{N|c_e|^2(1-|c_e|^2)}. \quad (20)$$

The projection noise vanishes when all the atoms are in one of the hyperfine levels, but in those cases the noise is dominated by other sources, such as the photon shot noise.

The signal-to-noise ratio for a projection noise limited measurement is

$$\frac{\mathcal{S}}{\mathcal{N}_P}=2\frac{A_{E1}t_R}{\hbar}\sqrt{N}. \quad (21)$$

Taking A_{E1} from Eq. (16), $t_R=1$ s, and integrating over 10^4 cycles, we would reach a 3% measurement with only 300 atoms.

The high-efficiency MOT that we developed at Stony Brook, with production rates around 10^6 s^{-1}, captures in excess of 10^5 francium atoms [28]. We expect to trap 10^6 atoms after transferring them to an ultrahigh vacuum environment. In this case, Eq. (21) predicts a signal-to-noise ratio of 20 in 1 s. Higher francium production rates could be obtained at other facilities, such as ISAC at TRIUMF, where an actinite target could deliver in excess of 10^8 atoms per second of a single isotope.

While measurements in francium benefit from a large A_{E1}, large atomic samples of other alkali-metal atoms are easily prepared. We could obtain the same signal-to-noise ratio in a cesium sample with 100 times more atoms and the same strength-driving field. While the fundamental signal-to-noise ratio indicates the inherent trade-offs between different alkali species, technical noise, specific to the instruments dedicated

TABLE II. Phase ($P=A/|A|$) of the relevant transition amplitudes for the initial state $F_1=4$, m_1 and final state $F_2=5$, m_2 and polarized along the specified axis. For this table all the fields have the same phase (equal to 0). P_{Rx} represents the Raman transition with one vector along the y axis and the other along the z axis, such that their cross product points along the x axis. β represents the static magnetic field reversal together with a sign change on the Zeeman sublevel m.

Reversal	m_1	m_2	P_{E1x}	P_{M1x}	P_{M1y}	P_{Rx}	P_{Ry}
Normal	0	−1	i	1	i	i	1
β	0	1	$-i$	−1	i	$-i$	1

to the measurement, must also be considered. For a discussion of technical noise in the cesium PNC Boulder experiment see Ref. [4].

IV. NOISE AND SYSTEMATIC EFFECTS

The measurement of the anapole moment would come from determining the population transferred from the lower to the upper hyperfine level by the application of the Raman and microwave fields. Both of these fields (or any other stray field) are characterized by a field amplitude, frequency (or detuning), and interaction time. The total transition amplitude for a common detuning (δ) and interaction time (t_R) is

$$A = (A_{R1} + A_{E11} + A_1) + i(A_{R2} + A_{E12} + A_2), \tag{22}$$

where $A_{R1,R2}$ are the real and imaginary components of the Raman amplitude, $A_{E11,E12}$ the corresponding for the $E1$ transition amplitude, and $A_{1,2}$ are the real and imaginary parts of any other transition present such as an $M1$ transition.

Table II shows the phase of the transitions for given field polarizations, with their transformation under magnetic field reversal assuming all the excitation fields are in phase. We control the phase difference (ψ) between the Raman field and the cavity $E1$ field. Varying ψ introduces an additional factor of $e^{i\psi}$ on the $E1$ transition amplitude while the Raman transition remains unchanged. The standing wave $M1$ field inside of the cavity is 90° out of phase with the $E1$ field, which gives a factor of $ie^{i\psi}$ for the $M1$ transition. If instead the $M1$ field corresponds to a traveling wave, then it is in phase with the $E1$ field.

The Raman field would be polarized along the y axis so that $A_{R1}=A_{Ry}$, and the $E1$ transition polarized along the x axis so that $A_{E11}=iA_{E1x}$ (or $\psi=\pi/2$). These two amplitudes would interfere since both are in phase and only one (the $E1$) changes sign under magnetic field reversal as shown in Table II. Expanding Eq. (12) for large A_{Ry} compared to the detuning and other amplitudes, we obtain

$$\Xi/N \simeq \sin^2\left(\frac{A_{Ry}t_R}{2\hbar}\right) + \frac{1}{2}\sin\left(\frac{A_{Ry}t_R}{\hbar}\right)\left(\frac{A_{ef}t_R}{\hbar}\right), \tag{23}$$

with

$$A_{ef} = \left(iA_{Ex} + A_1 + \frac{\hbar^2\delta^2}{2A_{Ry}} + \frac{1}{A_{Ry}}(A_{Rx} + A_2)^2\right). \tag{24}$$

A_{ef} contains the signal (A_{Ex}) and noise (A_1, A_2, A_{Rx}, and δ) terms. We can use this expression to set limits in the different experimental parameters and identify the corresponding observable. Expanding the last term in Eq. (23) for small t_R gives

$$\frac{t_R^2}{2\hbar^2}A_{Ry}A_{ef}. \tag{25}$$

The first term in A_{ef} is proportional to $iA_{Ry}A_{E1x}$, which corresponds to the PNC signal $i(\mathbf{E}\times(\mathbf{E}_{R1}\times\mathbf{E}_{R2})\cdot\mathbf{B})$.

The amplitudes of interest are the Raman amplitudes $A_{Rx,Ry}$, the $E1$ amplitude A_{E1x}, a $M1$ transition that is in phase with the $E1$ field $A_{Mix,Miy}$, and an $M1$ transition that is $\pi/2$ out of phase with the $E1$ field $A_{Mox,Moy}$. As an example, if the standing wave magnetic field inside of the cavity is tilted towards the x axis it generates an amplitude A_{Mox} since this field is out of phase with the $E1$ field. The $M1$ amplitudes are included in Eq. (24) as A_1 or A_2 depending on their phase relation to A_{Ry}.

The relevant values for the relative phase (ψ) between the $E1$ and the Raman transition are multiples of $\pi/2$. First we study the case with $\psi=0,\pi$. This does not correspond to the PNC measurement since the $E1$ and Raman transitions are out of phase and do not interfere. The signal obtained with this configuration is still helpful in the evaluation of unwanted contributions. We can rewrite A_{ef} from Eq. (24) using Table II and ignoring the detuning (δ) as

$$A_{ef} = \frac{1}{A_{Ry}}[(A_{Mox}^2 - A_{Miy}^2 - A_{Rx}^2) + s(iA_{Ry}A_{Moy} - 2iA_{Rx}A_{Mox}) + \beta(-2iA_{Miy}A_{Mox}) + s\beta(A_{Ry}A_{Mix} - 2A_{Miy}A_{Rx})], \tag{26}$$

with $s=1,-1$ when $\psi=0,\pi$, respectively, and $\beta=1,-1$ depending if we have the normal experiment or we apply a magnetic field reversal. With $\psi=\pi/2,-\pi/2$ instead we get

$$A_{ef} = \frac{1}{A_{Ry}}[(A_{Mix}^2 - A_{Rx}^2 - A_{Moy}^2) + s(iA_{Ry}A_{Miy} + 2iA_{Rx}A_{Mix}) - \beta(-2iA_{Moy}A_{Mix}) + s\beta(2A_{Rx}A_{Moy} - A_{Ry}A_{Mox} + iA_{Ry}A_{E1x})], \tag{27}$$

where now $s=1,-1$ when $\psi=\pi/2,-\pi/2$, respectively. This corresponds to the experimental condition for the PNC measurement. The PNC signal is contained in the last term, and it changes sign under both reversals. Equations (26) and (27) show how reversals can be used to isolate the PNC signal.

We divide the analysis of the different experimental parameters into three parts: Systematic effects that include terms that mimic the PNC signal and that are contained in the last parentheses of Eq. (27), line broadening mechanisms, which contain all other terms and that average to zero after an infinite number of cycles, and calibration errors that modify the value of the extracted constants on the PNC signal.

A. Line broadening mechanisms

We start with terms that do not change under both reversals. They include the detuning term from Eq. (24) and all the terms in Eq. (27) except for the last parentheses. We present the requirements to achieve a precision of 3% in the measurement after 10^4 repetitions. Each noise amplitude must be controlled to $3A_{E1}$

We could reduce the effect of some noise terms by increasing A_{Ry} [see Eq. (24)]. We would take A_{Ry} to be exactly equal to a $(2n+1)\pi/2$ pulse, and include any deviation from this value into A_1. We would control the Raman pulse to 0.025% in one second with shot noise limited detection. This would limit the maximum value for the Raman pulse to $A_{Ry}/\hbar=121$ rad/s or $n=38$. We now proceed to analyze the spurious terms in Eq. (27) that contaminate the signal.

1. $\hbar^2\delta^2/2A_{Ry}$

The detuning can have its origin in poor frequency control on the microwave or Raman fields, or changes in the external fields that shift the energy levels. The detuning would have to be controlled to $\delta=2.7$ rad/s. The required accuracy for the microwave field frequency is one part in 10^{11}.

Control of the static magnetic field B_0 to a fractional stability of 5×10^{-5} would keep the detuning under control.

The presence of an $M1$ transition produces an ac shift of the levels. The value of the maximum shift is ~3 mHz, which is negligible.

The atoms in the trap occupy different vibrational levels. Transitions between different vibrational levels are suppressed for a sufficiently far detuned trap. Each vibrational level has slightly different resonance frequency that leads to broadening of the signal and loss of coherence.

Coherence times as long as 4.4 s have been measured for atoms in a blue detuned trap [41]. The main source for decoherence was the distribution of Stark shifts felt by the atoms. We expect a coherence time 16 times smaller in francium than in Ref. [41] using a laser at 532 nm because of the difference in hyperfine splitting and detuning. The dephasing grows slowly in time and can be reversed with the use of an "echo" technique. The atoms would spend approximately one-half of the time in each hyperfine level with a Raman transition amplitude $A_R=(2n+1)\pi/2$ for large n. It is necessary in that case to keep the coherence for a time approximately equal to t_R/n, with t_R the duration of the experiment. We would need a coherence time of 26 ms for $n=38$ to have an interaction time of 1 s. This is below the expected 300 ms coherence time.

The average differential Stark shift seen by the atoms would be approximately equal to $kT(\Delta_{\mathrm{hfs}}/\delta)/h=6.3$ Hz. The effect of the time varying detuning generated by the oscillations in the trap is similar to a steady state detuning of the same magnitude, and can be compensated by adjusting the microwave frequency. We must control the power of the trap laser to 7%.

2. A_{Rx}^2/A_{Ry}

This term appears due to a bad polarization alignment of the Raman field. Control of the polarization of the Raman field to one part in 10^3 would be necessary to suppress this term.

3. $(A_{Mix}^2, A_{Moy}^2, A_{Rx}A_{Mix}, A_{Moy}A_{Mix})/A_{Ry}$

These terms are multiplied by a small number and their contribution becomes negligible. For example, $A_{Rx}A_{Mix}/A_{Ry}$ has the small factor A_{Rx}/A_{Ry} appearing due to polarization misalignment in the Raman beams.

4. $A_{Ry}A_{Miy}/A_{Ry}=A_{Miy}$

This is the dominant term that depends on the $M1$ transition. The $M1$ field appears due to imperfections in the microwave cavity field that create a traveling wave component that may be in or out of phase with the $E1$ transition.

Equation (18) gives the amplitude of the traveling wave expected in our setup. The traveling wave is polarized along the z axis, so we can include the polarization suppression factor of 10^{-3}. Combining these two numbers with the amplitude for the $M1$ transition we get an amplitude of $0.25A_{E1}$ out of phase with the $E1$ transition, and an in-phase amplitude of $0.75A_{E1}$.

The relative phase between both antennas (ϑ) can be adjusted by minimizing the $M1$ contribution when the static magnetic field $(\mathbf{B})$ is tilted slightly. The antennas phase mismatch contribution remains controlled for $\vartheta<0.01$ rad.

B. Systematic effects

The systematic effects include the terms in the last parentheses in Eq. (27). They change sign under both s and β reversals just as the PNC signal. The constraints for these terms are stronger since they do not average to zero. Their contribution must be below $0.03A_{E1}$ to reach a 3% measurement. We proceed to analyze each one of these terms.

1. $A_{Rx}A_{Moy}/A_{Ry}$

This term appears because of a combination of misalignment of the Raman field and misalignment of the microwave field or imperfections in the microwave cavity. It corresponds to the observable $\mathbf{M}\times(\mathbf{E}_{R1}\mathbf{E}_{R2})\cdot\mathbf{B}$. This term is reduced by the Raman misalignment (A_{Rx}/A_{Ry}) and its contribution would become negligible.

2. $A_{Ry}A_{Mox}/A_{Ry}=A_{Mox}$

This term has the same origin as the previous one, but its contribution is considerably larger since it is not suppressed by the Raman misalignment. It gives the limiting factor in the precision of the measurement and its control depends completely on the suppression mechanisms.

The cavity mirrors may have some birefringence, which generate a microwave magnetic field x-axis component. The microwaves make roughly 1000 reflections in the cavity. We need a polarization rotation smaller than 10^{-3} rad or a rotation per reflection smaller than 10^{-6} rad to keep the $M1$ suppression unchanged. The constraint for a 3% measurement is 14 times smaller.

The atomic sample would have to be precisely held at the node of the microwave magnetic field. The maximum dis-

TABLE III. Fractional stability required for a 3% measurement. The observable associated with each constraint is also included.

Observable	Constraint	Set value	Stability
$A_{Ry}A_{E1}$	Microwave amplitude	476 V/cm	0.03
$A_{Ry}A_{Ry}$	Raman amplitude	121 rad/s	2.5×10^{-4}
$(\hbar\delta)^2$	Microwave frequency	45 GHz	10^{-11}
	Dipole trap Stark shift	6.3 Hz	0.07
	dc magnetic field	1500 G	4.7×10^{-5}
$A_{Rx}A_{Rx}$	Raman polarization	0 rad	10^{-3} rad
$A_{Ry}A_{Miy}$	Mirror separation	13 cm	7.7×10^{-7}
	Antenna power	57 mW	0.02
	Antenna phase	0 rad	0.01 rad
$A_{Ry}A_{Mox}$	Mirror birefringence	0 rad	1×10^{-4} rad
	Trap displacement	0 m	3×10^{-11} m

placement we can tolerate is 3×10^{-11} m for a 3% measurement.

C. Calibration errors and requirements on theoretical calculations

The PNC signal [Eq. (13)] would give directly the A_{E1} amplitude since the uncertainty in the Raman amplitude is negligible. A_{E1} is the product of the microwave electric field and the matrix element. The microwave electric field amplitude must be known to 3%. The electric field could be measured by tilting the magnetic field and inducing an $M1$ transition. The extraction of information about the weak interaction from an experimental measurement requires theoretical input [24,42]. The quality of the electronic wave functions is the most important. The accuracy of the matrix elements must be comparable to that of the experiment. The effective constant of the anapole moment κ_a is obtained after subtracting the other two contributions to κ_i [Eq. (2)]. Johnson *et al.* show that the other contributions for the case of Fr amount to a few percent [27]. The anapole moment of the even-neutron isotopes comes only from the unpaired proton, while the odd-neutron isotopes contain contributions from the unpaired proton and neutron. A measurement of the anapole moment to better than 10% would give an initial separation of both contributions [22].

D. Other sources of fluctuations

The microwave magnetic field would generate transitions to other levels of the type $\Delta m=0$, which are nonresonant at the proposed magnetic field (detuning $\sim$0.4 GHz). Nevertheless, these transitions will have to be taken into account in a detailed analysis of the data.

Stray electric fields produce Stark induced transitions that mimic the PNC signal. A stray electric field of 13 V/cm in the z direction would generate a transition amplitude equal to the parity violating signal. Stray fields large enough to be a problem are unlikely to occur and can be ignored [29].

Gradients induce higher order multipole transitions, such as an $E2$ transition. Fortunately, these higher order transitions between the two hyperfine ground levels are strongly suppressed. Table III summarizes the results of the analysis of noise and systematic effects.

V. CONCLUSION

The anapole moment provides a unique probe of weak hadronic interactions. In particular it is sensitive to weak long-range meson exchange interactions, and consequently allows a measurement of weak neutral currents in the nucleus. This is not the case in high-energy experiments where the weak contribution must be separated from the strong and electromagnetic contributions that are much larger. We have presented the analysis of a proposed measurement strategy of the nuclear spin-dependent part of the PNC interaction, dominated by the anapole moment. While the proposed measurement method can be extended to other alkali-metal atoms, a series of measurements in a chain of francium isotopes allows the separation of the proton and neutron contributions to the anapole moment.

As noted by Fortson *et al.* [9,10] studies of atomic parity nonconservation give information on the nuclear physics. The nuclear weak interaction at low energies is often parametrized by a series of coupling constants, either with a meson exchange formalism, the so-called DDH parametrization [43], or more recently with effective field theories (EFT) [44]. A program of measurements of the anapole moment in a chain of francium isotopes will contribute significantly to constrain some of the DDH parameters, which together with the EFT program will provide a model independent input for theoretical analysis of low energy weak interaction constants. It is important to note that the measurement of the anapole moment of an even and an odd isotope of francium give almost orthogonal bands in the meson coupling parameter space. This is subject to the assumption that the anapole moment is carried mainly by the last nucleons [22], but as shown by the measurements of the hyperfine anomaly [7], this is a reasonable assumption. These measurements will significantly contribute to deepen our understanding of the nuclear structure.

ACKNOWLEDGMENTS

Work supported by NSF. One of the authors (E.G.) acknowledges support from CONACYT.

[1] Y. B. Zel'dovich, Sov. Phys. JETP **6**, 1184 (1958).
[2] V. V. Flambaum, I. B. Khriplovich, and O. P. Sushkov, Phys. Lett. **146B**, 367 (1984).
[3] P. A. Vetter, D. M. Meekhof, P. K. Majumder, S. K. Lamoreaux, and E. N. Fortson, Phys. Rev. Lett. **74**, 2658 (1995).
[4] C. S. Wood, S. C. Bennett, J. L. Roberts, D. Cho, and C. E. Wieman, Can. J. Phys. **77**, 7 (1999).
[5] C. S. Wood, S. C. Bennett, D. Cho, B. P. Masterson, J. L. Roberts, C. E. Tanner, and C. E. Wieman, Science **275**, 1759 (1997).
[6] A. Derevianko and S. G. Porsev, Phys. Rev. A **65**, 052115 (2002).
[7] J. S. Grossman, L. A. Orozco, M. R. Pearson, J. E. Simsarian, G. D. Sprouse, and W. Z. Zhao, Phys. Rev. Lett. **83**, 935 (1999).
[8] E. Gomez, L. A. Orozco, and G. D. Sprouse, Rep. Prog. Phys. **66**, 79 (2006).
[9] E. N. Fortson, Y. Pang, and L. Wilets, Phys. Rev. Lett. **65**, 2857 (1990).
[10] S. J. Pollock, E. N. Fortson, and L. Wilets, Phys. Rev. C **46**, 2587 (1992).
[11] C. E. Loving and P. G. H. Sandars, J. Phys. B **10**, 2755 (1977).
[12] V. G. Gorshkov, V. F. Ezhov, M. G. Kozlov, and A. I. Mikhailov, Sov. J. Nucl. Phys. **48**, 867 (1988).
[13] D. Budker, in *Physics Beyond the Standard Model*, edited by P. Herczeg, C. M. Hoffman, and H. V. Klapdor-Klinfrothaus (World Scientific, Singapore, 1998).
[14] V. E. Balakin and S. I. Kozhemyachenko, JETP Lett. **31**, 297 (1980).
[15] V. N. Novikov and I. B. Khriplovich, JETP Lett. **22**, 74 (1975).
[16] E. A. Hinds and V. W. Hughes, Phys. Lett. **67B**, 487 (1977).
[17] E. G. Adelberger, T. A. Trainor, E. N. Fortson, T. E. Chupp, D. Holmgren, M. Z. Iqbal, and H. E. Swanson, Nucl. Instrum. Methods **179**, 181 (1981).
[18] N. Fortson, Phys. Rev. Lett. **70**, 2383 (1993).
[19] M. V. Romalis and E. N. Fortson, Phys. Rev. A **59**, 4547 (1999).
[20] C. Chin, V. Leiber, V. Vuletic, A. J. Kerman, and S. Chu, Phys. Rev. A **63**, 033401 (2001).
[21] E. J. Angstmann, T. H. Dinh, and V. V. Flambaum, Phys. Rev. A **72**, 052108 (2005).
[22] V. V. Flambaum and D. W. Murray, Phys. Rev. C **56**, 1641 (1997).
[23] I. B. Khriplovich, *Parity Non-Conservation in Atomic Phenomena* (Gordon and Breach, New York, 1991).
[24] W. C. Haxton and C. E. Wieman, Annu. Rev. Nucl. Part. Sci. **51**, 261 (2001).
[25] R. R. Lewis, Phys. Rev. A **48**, 4107 (1993).
[26] The anapole moment operator is given by $\hat{\mathbf{a}}=(\pi e/m)[\mu(\mathbf{r}\times\sigma)-(q/2)(\mathbf{p}r^2+r^2\mathbf{p})]$, see for example, Ref. [21]. The anapole interaction for a spin-1/2 system is given by the Lagrangian $\mathcal{L}_a=(a/M^2)\bar{\psi}(x)\gamma_\mu\gamma_5\psi\partial_\nu F^{\mu\nu}$, see for example, J. Erler and M. J. Ramsey-Musolf, Prog. Part. Nucl. Phys. **54**, 351 (2005).
[27] W. R. Johnson, M. S. Safronova, and U. I. Safronova, Phys. Rev. A **67**, 062106 (2003).
[28] S. Aubin, E. Gomez, L. A. Orozco, and G. D. Sprouse, Rev. Sci. Instrum. **74**, 4342 (2003).
[29] D. DeMille and M. G. Kozlov, Phys. Rev. A (to be published).
[30] A. Coc, C. Thibault, F. Touchard, H. T. Duong, P. Juncar, S. Liberman, J. Pinard, J. Lermé, J. L. Vialle, S. Büttgenbach, A. C. Mueller, A. Pesnelle, and the ISOLDE Collaboration, Phys. Lett. **163B**, 66 (1985).
[31] A. Coc, C. Thibault, F. Touchard, H. T. Duong, P. Juncar, S. Liberman, J. Pinard, M. Carre, J. Lerme, J. L. Vialle, S. Büttgenbach, A. C. Mueller, A. Pesnelle, and the ISOLDE Collaboration, Nucl. Phys. A **468**, 1 (1987).
[32] S. Ramo, J. F. Whinnery, and T. V. Duzer, *Fields and Waves in Communication Electronics* (Wiley, New York, 1993).
[33] S. G. Porsev and M. G. Kozlov, Phys. Rev. A **64**, 064101 (2001).
[34] C. Bouchiat and C. A. Piketty, Phys. Lett. B **269**, 195 (1991).
[35] U. Harbarth, J. Kowalski, R. Neumann, S. Noehte, K. Scheffzek, and G. Z. Putlitz, J. Phys. E **20**, 409 (1987).
[36] J. W. Dees and A. P. Sheppard, IEEE Trans. Instrum. Meas. **14**, 52 (1965).
[37] V. I. Balykin, V. G. Minogin, and V. S. Letokhov, Rep. Prog. Phys. **63**, 1429 (2000).
[38] N. Friedman, A. Kaplan, and N. Davidson, Adv. At., Mol., Opt. Phys. **48**, 99 (2002).
[39] A. Kaplan, M. F. Andersen, and N. Davidson, Phys. Rev. A **66**, 045401 (2002).
[40] W. M. Itano, J. C. Bergquist, J. J. Bollinger, J. M. Gilligan, D. J. Heinzen, F. L. Moore, M. G. Raizen, and D. J. Wineland, Phys. Rev. A **47**, 3554 (1993).
[41] N. Davidson, H. J. Lee, C. S. Adams, M. Kasevich, and S. Chu, Phys. Rev. Lett. **74**, 1311 (1995).
[42] J. S. M. Ginges and V. V. Flambaum, Phys. Rep. **397**, 63 (2004).
[43] B. Desplanques, J. F. Donoghue, and B. R. Holstein, Ann. Phys. (N.Y.) **124**, 449 (1980).
[44] S. Zhu, C. M. Maekawa, B. R. Holstein, M. J. Ramsey-Musolf, and U. van Kolck, Nucl. Phys. A **748**, 435 (2005).